Anisotropy in the wetting of rough surfaces

Yong Chen, Bo He, Junghoon Lee, Neelesh A. Patankar *

Department of Mechanical Engineering, Northwestern University, 2145 Sheridan Road, Evanston, IL 60208-3111, USA

Received 29 March 2004; accepted 21 July 2004

Abstract

Surface roughness amplifies the water-repellency of hydrophobic materials. If the roughness geometry is, on average, isotropic then the shape of a sessile drop is almost spherical and the apparent contact angle of the drop on the rough surface is nearly uniform along the contact line. If the roughness geometry is not isotropic, e.g., parallel grooves, then the apparent contact angle is no longer uniform along the contact line. The apparent contact angles observed perpendicular and parallel to the direction of the grooves are different. A better understanding of this problem is critical in designing rough superhydrophobic surfaces. The primary objective of this work is to determine the mechanism of anisotropic wetting and to propose a methodology to quantify the apparent contact angles and the drop shape. We report a theoretical and an experimental study of wetting of surfaces with parallel groove geometry.
© 2004 Elsevier Inc. All rights reserved.

1. Introduction

Amplification of hydrophobicity due to surface roughness is frequently seen in nature [1] and has been demonstrated for microfabricated rough surfaces [2–4]. Roughness induced superhydrophobicity is considered a viable option for surface tension induced drop motion in microfluidic devices. Another application is inspired by superhydrophobic plant leaves. Water drops are almost spherical on some plant leaves and can easily roll off, cleaning the surface in the process [1]. There are numerous applications of artificially prepared 'self-cleaning' surfaces.

A drop can typically reside in two ways on a given rough hydrophobic surface [3–7]. It either sits on the peaks of the surface roughness or wets the grooves (to be referred to as a wetted contact), depending on how it is formed. The energy of these two states is different—the one with a larger contact angle has higher energy [5,8]. Which of the two states has lower energy is determined by the geometry of the surface roughness [5,8]. A drop that sits on the peaks has 'air pockets' along its contact with the substrate; hence it will be termed a 'composite' contact. A drop with a composite contact is of interest because it easily moves on the substrate due to reduced resistance [9,10]. This is desirable in applications such as 'self-cleaning' surfaces [6].

If the roughness geometry is isotropic then the drop shape is almost spherical and the apparent contact angle of the drop with the rough surface is nearly uniform along the contact line. The apparent contact angle for a 'composite' spherical drop is given by Cassie's formula [11] while that for a 'wetted' spherical drop is given by Wenzel's formula [12].

If the roughness geometry is not isotropic, e.g., parallel grooves, then the apparent contact angle is no longer uniform along the contact line. It was reported that the apparent contact angles observed perpendicular and parallel to the direction of the grooves are different [3]. The exact mechanism for anisotropic wetting and the resultant shape of the drop were not discussed [3]. Anisotropic wetting for chemically patterned hydrophilic surfaces has also been observed [13]. Wenzel and Cassie formulas are insufficient to understand this anisotropy in the wetting of rough surfaces. A better understanding of this problem is critical in designing rough superhydrophobic surfaces. In this paper we report a theoretical and an experimental study of the wetting of surfaces with anisotropic roughness. The primary objective of this work is to determine the mechanism of anisotropic wetting

* Corresponding author.
E-mail address: n-patankar@northwestern.edu (N.A. Patankar).

and to propose a methodology to quantify the apparent contact angles and the drop shape.

In Section 2 we will present results based on numerical simulations to understand the primary characteristics of the drop shape on anisotropic roughness. In Section 3, we will present experimental results of contact angle measurements. The mechanism of anisotropic wetting will be discussed. A concept of 'equivalent' contact line will be used to theoretically reproduce the experimental results. Discussion and conclusions will be presented in Section 4.

2. Numerical simulation of the drop shape

Public domain software by Ken Brakke [14,15] is used to numerically investigate the 3D drop shapes and the apparent contact angles on rough surfaces. We consider a roughness geometry of horizontal grooves (Fig. 1). A similar investigation of drop shapes on chemically heterogeneous surfaces has been reported earlier by Brandon et al. [16,17]. We neglect gravity, which is a reasonable assumption for small drops.

The numerical procedure is based on minimizing the free energy of the system to obtain the equilibrium drop shape. The free energy G of the system is given by

$$\frac{G}{\sigma_{lf}} = S_{lf} - \iint\limits_{S_{sl}} \cos\theta_a \, dA, \tag{1}$$

where l denotes the liquid that makes the drop, f denotes the fluid (typically air) surrounding the drop, s denotes the solid surface, S_{lf} and S_{sl} are the liquid–fluid and the solid–liquid interfacial areas of contact and σ_{lf} is the liquid–fluid interfacial tension (or surface energy density). σ_{lf} is assumed to be constant. The intrinsic contact angle θ_a of the substrate material is defined by Young's equation,

$$\cos\theta_a = \frac{\sigma_{sf} - \sigma_{sl}}{\sigma_{lf}}, \tag{2}$$

where σ_{sl} and σ_{sf} are the local solid–liquid and solid–fluid interfacial tensions, respectively. $\theta_a > 90°$ represents a hydrophobic contact. The expression for the free energy can be appropriately modified to account for gravity. Minimizing the 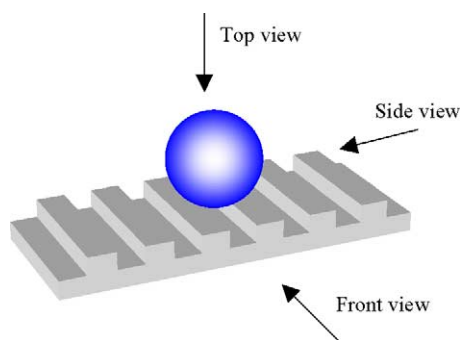free energy G (Eq. (1)) with respect to the liquid–fluid interface shape, while constraining the drop volume to a fixed value, gives the equilibrium drop shape. In the solution procedure, G/σ_{lf} is minimized. Hence, for a given problem, the only material parameter we need to specify is θ_a.

It can be shown [18] using variational principles that the constrained minimization procedure, above, is equivalent to solving the Laplace equation for the pressure drop at each point on the liquid–fluid interface,

$$\frac{2\sigma_{lf}}{R_m} = \Delta p, \tag{3}$$

along with Young's equation (2) on the solid–liquid–fluid contact line as the boundary condition. R_m is the mean radius of curvature and Δp is the pressure drop, at a point on the drop surface. A stationary drop on a substrate, in constant ambient pressure, will have a constant pressure drop at each point on the liquid–fluid interface (gravity neglected). Hence, it follows directly from Eq. (3) that a sessile drop should have a constant mean curvature surface. In two dimensions, the arc of a circle is the only constant mean curvature curve. In three dimensions, the spherical surface is one of the many possible constant mean curvature surfaces.

Detailed information about the numerical methodology to solve the constrained minimization problem (Eq. (1)) is available in the Surface Evolver manual [14]. A brief description is given here.

The equilibrium drop shape is obtained iteratively from the initial shape. At each iteration the vertices on the liquid–fluid interface are moved in order to reduce the energy of the system while adhering to the imposed constraints (e.g., constant volume). Iterations are repeated until the system's energy does not change significantly. Suitable modifications were done to the software to handle a rough substrate.

We consider a drop of a given volume placed on the rough substrate. We start with an initial drop shape (Fig. 2). The grooves underneath the drop are initially filled with liquid (Fig. 2). The intrinsic contact angle of the drop on the solid surface is specified. The Surface Evolver is used to obtain the final equilibrium drop shape from a given initial shape (Fig. 2).

Our objective here is to understand the general qualitative features of the drop shape. To this end we consider a drop of unit volume. The groove is 0.1 unit wide × 0.1 unit deep. The pillar width is also taken as 0.1 unit. Multiple equilibrium shapes can be obtained for the drop depending to the

Fig. 1. Schematic of a sessile drop on a substrate with horizontal grooves. Note the definitions of the different views.
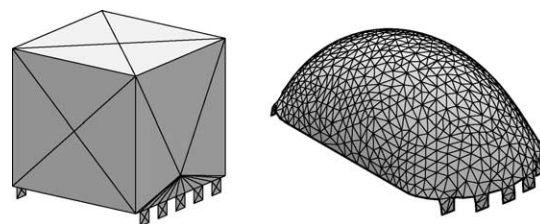

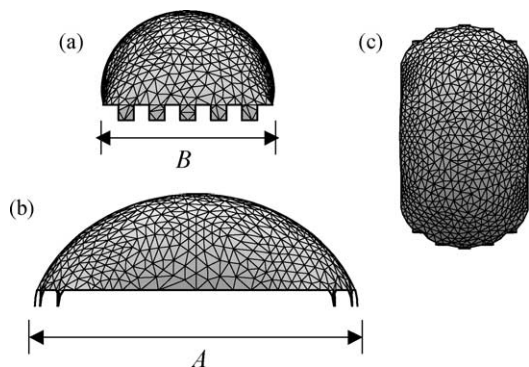Fig. 2. Initial and equilibrium configurations of a drop on six pillars. The intrinsic contact angle is 90°.

Fig. 3. (a) Front, (b) side, and (c) top views of the drop in Fig. 2. A and B are the lengths of the base of the drop in the side and front views, respectively.
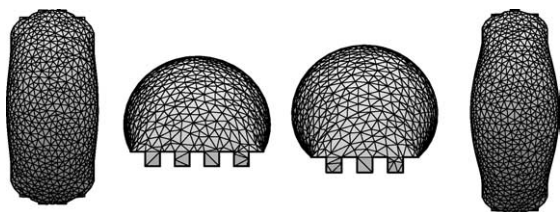

Fig. 4. Equilibrium drop shapes as a function of the number of pillars on which it settles. Two figures on the left are for five pillars and the two on the right are for four pillars (figures for the two cases are not drawn to the same scale).

number of pillars on which the drop resides [19]. During a given run we fixed the number of pillars on which a drop sits and find if an equilibrium shape is possible. Note that an equilibrium shape is not possible for any choice of the number of pillars underneath the drop.

Fig. 2 shows the initial shape (which is arbitrary) and the final equilibrium shape when the drop resides on six pillars. The left and the right edges of the drop are constrained to move on the first and the sixth horizontal pillars, respectively (see Fig. 2). The equilibrium shape thus obtained is the local minimum of the free energy. The resultant equilibrium shape satisfies the condition that the mean curvature of the surface is constant. The local contact angle along the actual solid–liquid–fluid contact line is equal to the intrinsic contact angle ($\theta_a = 90°$ in this case).

Fig. 3 shows the various views of the drop in Fig. 2. We see that the fluid 'pins' on the edge of the horizontal pillars. For an intrinsic contact angle of 90°, the apparent contact angle on the edge can vary between 90° and 180° (see Oliver et al. [20]). The apparent contact angles in the front and side are different (Fig. 3), in qualitative agreement with previous experiments [3]. We will report similar observations from our experiments to be discussed later in this paper. Note that the apparent contact angles are not equal to the intrinsic contact angle of 90°.

Fig. 4 shows the effect of the number of pillars on which the drop resides. All the other parameters, i.e., the drop volume, the liquid–fluid surface tension and the intrinsic contact angle, are the same as in the case in Fig. 2. The shape of the drop becomes longer as the number of pillars is reduced.
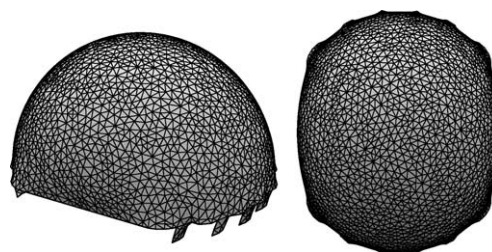

Fig. 5. Equilibrium drop shape for $\theta_a = 105°$. All other parameters are the same as the case in Fig. 2.
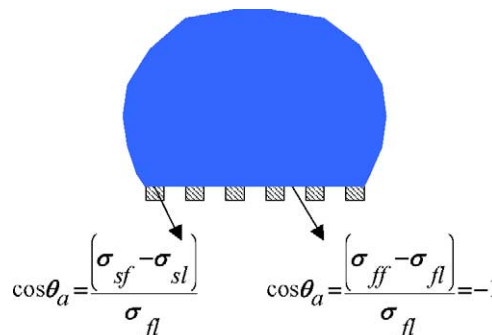

Fig. 6. A cartoon of the front view of a drop with a composite contact with a rough substrate with horizontal grooves.

The apparent contact angle increases in the front view as the number of pillars is reduced. In each case the left and the right edges are pinned on the edge of the horizontal pillars. Of the three cases considered here, the free energy of the drop sitting on six pillars (Fig. 3) is minimum. The drop can acquire any of the configurations above depending on how it is formed. Cases with more pillars were not considered in view of the computational cost.

In Figs. 2–4 we considered drops with wetted contacts; i.e., the grooves are filled with liquid. The qualitative features presented above remain typically unaltered for hydrophobic cases (i.e., $\theta_a > 90°$) if a wetted contact is formed (Fig. 5)

In this work we are mainly interested in hydrophobic drops with composite contacts with the substrate. In the later sections we will present experimental results for the composite contact case. The composite contact case can be set up for numerical simulations as depicted in Fig. 6.

Fig. 6 shows a cartoon of the front view of a drop on six pillars with a composite contact with the rough substrate. The assumptions involved are that the liquid–fluid interface on top of the empty grooves is almost flat. This is reasonable when the drop size is large so that the mean radius of curvature is large compared to the size of the roughness features. The problem is then equivalent to a drop on a heterogeneous (i.e., intrinsic contact angle changes) flat surface. On the horizontal pillars the intrinsic contact angle is same as that of the substrate material and at the location of the grooves the effective intrinsic contact angle is 180° (Fig. 6).

We solve the composite drop case using Surface Evolver. The intrinsic contact angle of the substrate material is taken
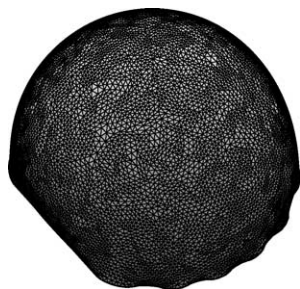
Fig. 7. The drop shape on a rough substrate for the composite contact case.

Table 1
Experimental data for drops of different volumes V on a rough surface of parallel groove geometry

V (mm^3)	θ_F (°)	θ_S (°)	$\Delta\theta$ (°)	A (mm)	B (mm)	Pillars
0.59	140.4	125.4	15	0.898	0.698	15
1.432	143.7	125	18.7	1.215	0.898	19
2.077	144.1	125.5	18.6	1.376	1.008	21
4.818	148.1	128	20.1	1.764	1.267	26
5.151	149.5	126.5	23	1.855	1.247	26
5.679	150.7	127.2	23.5	1.887	1.267	26

θ_F is the apparent contact angle in the front view, θ_S is the apparent contact angle in the side view and $\Delta\theta = \theta_F - \theta_S$. The number of pillars are estimated based on B and the pillar and groove dimensions.

to be 120°. The pillar and groove widths and the drop volume are the same as in the cases depicted in Figs. 2–4. Similar to the wetted drop case, there are multiple equilibrium shapes depending on the number of pillars on which the drop resides. Fig. 7 shows the drop shape for the case when there are six pillars underneath the drop. Once again we see pinning of the liquid at the edge of the pillars. The apparent contact angles in the front and side views are different and greater than 120°.

A few comments are in order. We have observed the pinning of the fluid at the edge of the pillars for the cases we have considered (a few of which are presented above). There is no guarantee that we have exhausted all the possible cases. Thus, pinning may not exist for all possible equilibrium shapes. However, we note that Surface Evolver simulations of Brandon et al. [17] for chemically patterned surfaces do show similar characteristics.

Based on the above we conclude that there are, as expected, multiple equilibrium shapes for a drop on a rough surface with parallel grooves. A particular equilibrium shape can be typically obtained by fixing the number of pillars on which the drop resides. For the case of a composite contact of a hydrophobic drop, the apparent contact angles in the front and side views are different and both are usually larger than the intrinsic value of the substrate material. In addition, the apparent angle in the front view is usually larger than the apparent angle in the side view (also see the next section). This is a consequence of the squeezing and pinning of the drop in the front view and stretching of the drop in the side view. Further discussion on this will follow in the next section.

3. Experimental observation of anisotropic wetting

We fabricated a rough substrate with a parallel groove geometry. The fabrication method is discussed by He et al. [4]. The substrate material was made of PDMS ($\theta_a = 114°$). The pillar width was 23 μm, the groove width was 25.6 μm and the pillar height (i.e., also the groove depth) was 30 μm. A droplet of specified volume was gently deposited on the substrate by an automatic pipette. This resulted in a composite contact [4]. The contact angles were then measured in the front and side views. We also measured the length of the base of the drop (see definitions in Fig. 3) in the front and side views. These measurements were done by a goniometer (AST Products Inc., VCA Optima XE, Boston, MA) that takes and analyzes images of sessile droplets on surfaces. The data are given in Table 1. Each case was measured after depositing a new drop.

In all cases the apparent contact angles in the two views are unequal and both are greater than the intrinsic contact angle of PDMS ($\theta_a = 114°$). The angle in the front view is larger than the angle in the side view; correspondingly the base length B in the front view is smaller than the base length A in the side view (Fig. 8).

The apparent contact angle θ_c for a spherical composite drop on this substrate can be calculated by Cassie formula [5,11]. For the geometric parameters given above we get $\theta_c = 136°$. This value is between θ_F and θ_S. The Cassie formula assumes a spherical drop with a circular contact line so that the apparent contact angle is uniform as seen from all
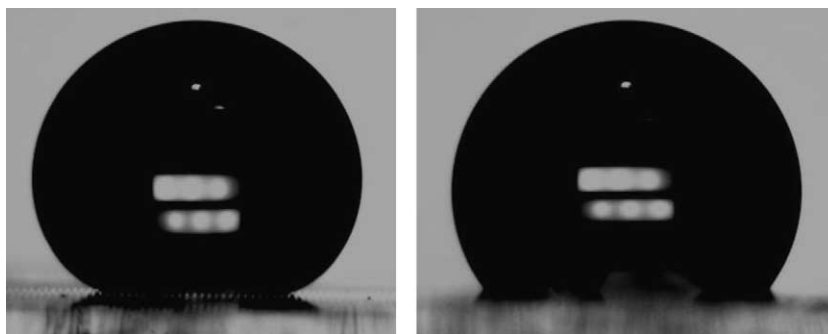

Fig. 8. Front (left) and side (right) views of a sessile drop on a rough surface with parallel groove geometry. It is evident from the front view that the drop is sitting on top of the pillars. The drop volume is 5.15 mm^3, $\theta_F = 149.5°$, $\theta_S = 126.5°$ and $B < A$.

Table 2
Comparison of D_{sp}, A, B and D for the experiments in Table 1

V (mm^3)	D_{sp} (mm)	A (mm)	B (mm)	D (mm)
0.59	0.736	0.898	0.698	0.798
1.432	0.989	1.215	0.898	1.057
2.077	1.12	1.376	1.008	1.192
4.818	1.48	1.764	1.267	1.516
5.151	1.52	1.855	1.247	1.551
5.679	1.566	1.887	1.267	1.577

directions. This is not the case here. The average shape of the contact line in this case is not circular since $A \neq B$. Thus, Cassie formula does not fully explain the observed behavior in Table 1.

The anisotropy in wetting can be explained based on the results presented in Section 2. To this end, consider a spherical composite drop on the rough substrate. The diameter D_{sp} of the circular contact line at the base of the spherical drop is given by

$$D_{sp} = 2\left(\frac{3V}{\pi(1 - \cos\theta_c)^2(2 + \cos\theta_c)}\right)^{1/3} \sin\theta_c, \qquad (4)$$

where V is the drop volume. In Table 2 we list the value of D_{sp} for different drop volumes in the experiment. For comparison, the values of A and B are listed again in Table 2. We also note that D_{sp} is a good estimate (within 7%) of the mean diameter, $D = (A + B)/2$, of the base of the drop (Table 2).

It is seen from Table 2 that D_{sp} is always greater than B while it is always less than A. This implies that the experimentally observed drop is such that it resides on fewer pillars compared to a spherical composite drop on the same substrate. Thus the base of the drop is 'squeezed' (Fig. 8) in the front view compared to a spherical composite drop on the same substrate ($B < D_{sp}$). The 'squeezing' is possible because the drop pins on the edge of the pillars as seen in the front view (Section 2). Due to squeezing and pinning, the apparent angle θ_F in the front view is larger than $\theta_c = 136°$ (which is itself larger than the intrinsic contact angle $\theta_a = 114°$ of the substrate material because of the presence of air in the grooves).

Since the drop is 'trapped' on fewer pillars, i.e., squeezed as seen in the front view, it leads to 'stretching' (Fig. 8) in the side view compared to a spherical composite drop on the same substrate ($A > D_{sp}$). This results in an elongated drop as simulated in Section 2. Stretching causes the apparent angle θ_S in the side view to be smaller than θ_c. Note that θ_S is still larger than the intrinsic contact angle of the substrate due to the presence of air.

The above two paragraphs qualitatively explain why θ_F and θ_S are greater than the intrinsic contact angle of the substrate material. The fact that $\theta_F > \theta_S$ is because the drop sits on fewer pillars compared to the number of pillars on which a spherical composite drop would sit on the same substrate. It is possible that θ_F would be less than θ_S if the drop somehow got trapped on more number of pillars compared to

the number of pillars on which a spherical composite drop would sit on the same substrate. We did not get this case experimentally. These conclusions are consistent with the results of Brandon et al. [17] for chemically patterned surfaces.

In Section 2 we have seen that different equilibrium drop shapes are obtained depending on the number of pillars on which a drop resides. We also saw that the fewer the pillars on which the drop resides, the greater the apparent angle in the front view. The experimental observations are consistent with the simulation results. The discussion here, although qualitative, highlights the mechanism of anisotropy in wetting.

Next, we obtain quantitative information regarding the apparent contact angles and the drop shape. One option is to perform simulations as in Section 2 for a composite drop on the substrate. The number of pillars on which the drops, in the experiments, reside range from 15 to 26. It is computationally very expensive to resolve the drop shape in such detail. We consider a different approach, which is discussed below.

At the microscopic scale the actual contact line of a drop on a rough substrate is not smooth. However, the actual contact line can be approximated, e.g., by an equivalent smooth circular contact line in the case of a spherical composite drop. This particular drop shape can be regarded as the one with the lowest energy among all the constant mean curvature surfaces of spherical shape [21]. This approximation works well for isotropic rough surfaces. For anisotropic rough surfaces, the drop can form a different mean curvature surface that is not spherical. In order to approximate such a shape we assume an equivalent smooth noncircular contact line along the base of the drop instead of resolving the details of the actual contact line. We can then find a constant mean curvature surface that has this specified noncircular contact line. The resultant shape will give the apparent contact angles in the front and side views.

We hypothesized different shapes for the equivalent contact line that matched the values A and B in the two views. An ellipse is one choice but we found that a cubic equation resulted in better agreement with the experimental data. The equation for the cubic contact line is

$$\left(\frac{2|x|}{A}\right)^3 + \left(\frac{2|y|}{B}\right)^3 = 1, \qquad (5)$$

where $|\ |$ denotes the positive value of the variable. For each of the experimental cases, we used the experimental values of A and B in the cubic equation above. This gave the equivalent contact line of the drop. Then we used Surface Evolver to find a constant mean curvature surface that has the specified contact line and the specified (experimental value) volume. The resultant drop shapes were long—similar to those in Section 2. The apparent contact angles in the side and front views were then calculated from the simulated drop shapes. Fig. 9 shows a comparison of the experimental and numerical values of θ_F and θ_S. We see that the agreement is
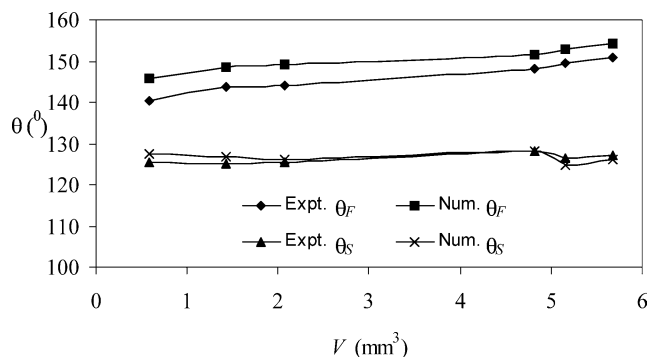
Fig. 9. Comparison of the experimental and numerical values of θ_F and θ_S.
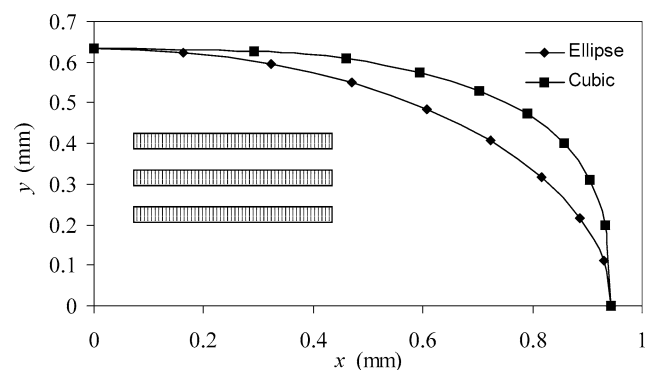

Fig. 10. Comparison of the elliptic and cubic shapes of the equivalent contact line for $A = 1.887$ and $B = 1.267$. The inset shows the direction of the pillars and grooves. The contact line is shown only in the first quadrant; it can be symmetrically reproduced in the remaining quadrants.

Fig. 11. Plot of $\Delta\theta$ as a function of ε for increasing values of V'. The plot is obtained from numerical simulations by assuming an elliptic contact line at the base of the drop.

Table 3
$\Delta\theta$, V' and ε for the experimental data points plotted in Fig. 9

V (mm^3)	$\Delta\theta$ (°) (expt.)	V'	ε
0.59	15	2.955	0.125
1.432	18.7	3.091	0.150
2.077	18.6	3.121	0.154
4.818	20.1	3.523	0.164
5.151	23	3.514	0.196
5.679	23.5	3.686	0.196

fairly good (within 10–15%) and consistent in terms of the trend. We note that a correct trend was obtained even with an elliptic contact line but the quantitative agreement with the experimental data was not very good. This indicates that the cubic curve for the equivalent contact line is a good approximation of the average shape of the actual contact line of the drop, at least for the parameter we have considered.

In Fig. 10 we compare the elliptic and cubic shapes of the equivalent contact line for $A = 1.887$ and $B = 1.267$ (last experimental date point in Tables 1 and 2). We note that the cubic line is 'flatter' on the sides, thus indicating a shape closer to the 'pinned' contact line seen in Section 2 above. This further corroborates the mechanism of anisotropic wetting as discussed above.

The trend in Fig. 9 can be understood better by considering the parameters that influence the value of $\Delta\theta$. Nondimensionalizing the variables of interest ($\Delta\theta$, V, A, B) we get $\Delta\theta = f(V', \varepsilon)$, where

$$V' = \frac{8V}{\pi D^3}, \qquad \varepsilon = \frac{A - B}{A + B}. \qquad (6)$$

V' is the nondimensional volume of the drop and ε is a nondimensional measure of the aspect ratio of the contact line of the drop. In Fig. 11 we plot $\Delta\theta$ as a function of ε for increasing values of V'. The plot is obtained from numerical simulations by assuming an elliptic contact line at the base
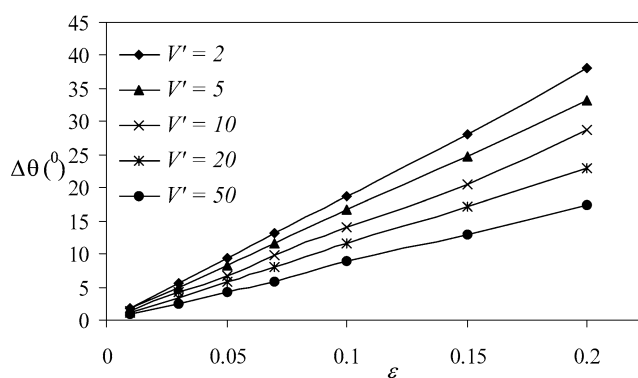
of the drop. The qualitative features for the cubic contact line will be the same. We see that $\Delta\theta$ increases with increasing ε. This is expected since larger values of ε imply a less spherical drop leading to greater anisotropy. Fig. 11 also shows that for the same value of ε, $\Delta\theta$ decreases as V' increases. The drop tends to be more spherical for larger volumes.

In Table 3 we list $\Delta\theta$, V' and ε for the experimental data points plotted in Fig. 9. The results in Fig. 11 readily shed light on the qualitative features of the changes in the value of $\Delta\theta$.

4. Discussion and conclusions

We conclude that there are, as expected, multiple equilibrium shapes for a drop on a rough surface with parallel grooves. A particular equilibrium shape can be typically obtained by fixing the number of pillars on which the drop resides. This helps to explain the anisotropy in the wetting of rough surfaces with parallel grooves.

We considered (theoretically and experimentally) a hydrophobic composite drop, i.e., a drop that does not wet the grooves of the rough surface. The apparent contact angles in the front and side views are different and both are larger than the intrinsic value of the substrate material. The drop is typically trapped in a state where it resides on fewer pillars compared to a spherical composite drop on the rough surface. As a result, the apparent angle in the front view is larger than the apparent angle in the side view. This is a con-

sequence of the squeezing and pinning of the drop in the front view and stretching of the drop in the side view.

We find that the experimental data are reproduced well numerically if we assume an equivalent smooth noncircular contact line along the base of the drop and find the corresponding constant mean curvature surface. The resultant drop shape is not spherical. The apparent contact angles in the front and side views are in good agreement with the experimental data.

It must be noted that the state of the drop we observe experimentally is not necessarily the lowest energy state. It only implies that the observed state is a local low energy state that is well separated from the 'neighboring' lower energy states by an energy barrier. Hence, it gets trapped in the observed state. Numerical simulations of Brandon et al. [17] for chemically patterned surfaces show that the shapes for which *A* and *B* are almost equal (i.e., shapes close to spherical) have the lowest energy among all the possible equilibrium states. The same is expected to be valid for the problem considered in this paper and is supported by our preliminary results not reported here. Thus the optimum number of pillars under the drop would correspond to the most spherical drop shape. A detailed investigation of this aspect can be done either by highly resolved simulations as outlined in Section 2 or by considering the approach of an equivalent noncircular contact line discussed in Section 3.

Yoshimitsu et al. [22] showed that the sliding properties of drops are different on anisotropic substrates such as those considered in this work. They showed that drops slide better when the grooves are parallel to the slope. This appears consistent with the conclusions of our work. Pinning of the fluid on the edge of the pillars will cause greater resistance to sliding when the grooves are perpendicular to the slope.

Acknowledgment

References

[1] W. Barthlott, C. Neinhuis, Planta 202 (1997) 1–8.
[2] T. Onda, N. Shibuichi, N. Satoh, K. Tsuji, Langmuir 12 (1996) 2125–2127.
[3] J. Bico, C. Marzolin, D. Quere, Europhys. Lett. 47 (1999) 220–226.
[4] B. He, N.A. Patankar, J. Lee, Langmuir 19 (2003) 4999.
[5] N.A. Patankar, Langmuir 19 (2003) 1249.
[6] N.A. Patankar, Langmuir 20 (2004) 8209.
[7] N.A. Patankar, Langmuir 20 (2004) 7097.
[8] A. Marmur, Langmuir 19 (2003) 8343.
[9] A. Lafuma, D. Quéré, Nat. Mat. 2 (2003) 457.
[10] B. He, N.A. Patankar, J. Lee, Colloids Surf. A (2004), in press.
[11] A.B.D. Cassie, Discuss. Faraday Soc. 3 (1948) 11.
[12] T.N. Wenzel, J. Phys. Colloid Chem. 53 (1949) 1466.
[13] H. Gau, S. Herminghaus, P. Lenz, R. Lipowsky, Science 283 (1999) 46.
[14] K.A. Brakke, http://www.susqu.edu/facstaff/b/brakke/evolver.
[15] K.A. Brakke, Exp. Math. 1 (1992) 141.
[16] S. Brandon, A. Wachs, A. Marmur, J. Colloid Interface Sci. 191 (1997) 110.
[17] S. Brandon, N. Haimovich, E. Yeger, A. Marmur, J. Colloid Interface Sci. 263 (2003) 237.
[18] R. Finn, Equilibrium Capillary Surfaces, Springer-Verlag, 1986, pp. 4–10.
[19] R.E. Johnson, R.H. Dettre, Adv. Chem. Ser. 43 (1963) 112.
[20] J.F. Oliver, C. Huh, S.G. Mason, J. Colloid Interface Sci. 59 (1977) 568.
[21] G. Wolanski, A. Marmur, Colloids Surf. A 156 (1999) 381.
[22] Z. Yoshimitsu, A. Nakajima, T. Watanabe, K. Hashimoto, Langmuir 18 (2002) 5818.